
UNIVERSITY OF THESSALY

SCHOOL OF ENGINEERING

DEPARTMENT OF ELECTRICAL AND COMPUTER ENGINEERING

# TIME DOMAIN INDEX MODULATION (IM) IN A DIGITAL COMMUNICATION SYSTEM

Zervos Spiridon
spiridonzervos@gmail.com

# Time domain Index Modulation (IM) in a residual carrier digital communication system

**Abstract**

The wireless network of today is the result of constantly increasing demands in the area of wireless communication. It's value is visible at both an individual and a societal level and can be noticed by the rate of usage as well as from the new needs that arise from it. Whereas wireless technology is evolving at an ever growing pace, it's progress is slowly coming at a halt due to the spectrum crunch, all the while demanding new technologies such as the Internet of Things, is pressing for ever larger rates and quantities in wireless transmissions. To tackle this obstacle, new techniques have been introduced to the status quo, one of which being the scheme of Index Modulation (IM). IM provides additional information by introducing activation states to the communication medium, thus offering a variety of integration methods. In the scope of this study, we focus on Time slot Index Modulation applied on a SISO (single-input single-output) wireless communication channel between transmitter and receiver. Furthermore, a residual carrier is used for transmitting the data signal, as well as a Phase-Locked Loop component by the receiver to undo the channel's attenuation. Last but not least, the results of the experiment are presented and comparisons are made between the proposed scheme and currently used ones.

# Table of Contents

# List of Figures and Tables

# CHAPTER 1: INTRODUCTION

With the advancement of technology, wireless transmission has become a key component in human activity and daily life. Mobile phones, WiFi and signal transmissions in general are prime examples of applied wireless techniques. Moreover, advancements in both hardware and software technologies, have further integrated said techniques as a basis of many applications [1],[2], the most recent of them being the Internet of Things (IoT) [3], which will further increase the demand for higher data rates and sizes.
The need for bigger quantities in data sizes and higher transmission speeds in combination with the limitations imposed by the spectrum crunch phenomenon [4] has led to new techniques and methods in wireless communication to tackle such issues. The wide range of these new methods offer promising results with reduced bandwidth requirements. As an example, in [5], the authors insert the term Heterogeneous Networks (HetNets) which offer increased capabilities due to better spectrum management than the microwave based networks that are currently used. In [6], a Light Fidelity (LiFi) system is established for the creation of a wireless network; LED and LDs are used as transmitters and receivers, thus using the optical spectrum for transmission.
Other techniques focus on achieving the specifications of IoT. The authors of [7], state that OFDM, a modulation scheme extensively used in most modern-day applications, cannot fully meet the requirements of 5G. This is further backed up in [8], where modifications of the OFDM scheme lead to reduced overall errors in the transmission sessions. In [9], with the usage of Reconfigurable Intelligent Surfaces (RIS) as a basis for the transmission scheme, higher data rates were achieved, while it was also stated that they could be integrated in beyond MIMO (multiple-input multiple-output) topologies.

## 1.1 Index Modulation

In the context of new methods and techniques developed for wireless communication, the scheme of Index Modulation (IM) is proposed. IM has been the subject of an increasing amount of studies over the years due to it's positive results in it's various applications, especially in achieving the demands of 5G networks [10]; this stems from the fact that the IM scheme encodes information within the states of the transmission medium. In addition, since it's integration alters the physical layer (PHY) of the OSI layer stack, it can be used in conjunction with other modulations, further increasing their robustness.

## 1.2 Literature Review

The encoding of information in the medium of the transmission, as well as the freedom to implement IM with other modulations, offer a great amount of flexibility in it's applications. Depending on the requirements of each transmission scenario, the appropriate medium is selected. The variability in the choice of the medium has lead to various IM schemes such as Spatial Modulation (SM) in MIMO systems taking advantage of the multi-channel nature of the topology, OFDM-IM [8] where additional information is encoded in the sub-carriers of the transmission, Time slot IM where the transmission time is divided into time slots which are then used for the additional information. The flexibility in IM's application offers adaptability depending on the demands, resulting in different schemes or hybrid ones with positive results presented in [6], [11], [12], [13], [14].
In addition, according to the authors of [11], IM is a subclass of the Permutation Modulation (PM) introduced by Slepian D. in [15]. According to PM, a permutation vector is used by the

transmitter (TX), which defines the alphabet of the modulation; the receiver (RX) then can decode the information based on the alphabet. In IM, the permutation vector regards the state activation of the medium that is chosen.

## 1.3 Purpose of Dissertation

As it was mentioned above, IM has a vast amount of flexibility in it's application and thus a variety of studies have used it as a key component. Since, MIMO systems are the principle of today's wireless transmission systems, as they take advantage of the multi-channel nature of the wireless equipment [16], IM's applications focus on this nature in combination with the OFDM scheme. On the other hand, where a different approach is introduced, IM's application greatly alters the TX-RX model of communication. In this dissertation we focus on the scheme of Time slot Index Modulation in a SISO system. Furthermore, a single residual carrier signal is used, as well as a Phase-Locked Loop (PLL) component to undo the channel's attenuation on the transmitted signal.

## 1.4 Dissertation Structure

The present dissertation is divided into seven chapters. In chapters 2 through 4, the main components of the model are introduced and analysed; in Chapter 2, TX as well as the application of Time slot Index Modulation scheme is studied. Chapter 3 examines the transmission channel and it's effects on the transmitted information signal, while the RX of our model is introduced in Chapter 4 alongside with the effects of Time slot Index Modulation on the reception of the signal. In Chapter 5, the model's topology is presented as well as the algorithms that were developed for each component, including the calculation of the Bit Error Rate (BER). The results of the study are shown in Chapter 6 for different Signal-to-Noise Ratio (SNR) and Carrier-to-Noise Ratio (CNR) values. Lastly, in Chapter 7, we summarize the results and mention prospects for future studies.

# CHAPTER 2: TRANSMITTER

## 2.1 TX Topology

In this chapter, the transmitter's topology is presented and then analyzed in it's respective components. TX's topology is displayed in Figure 1:

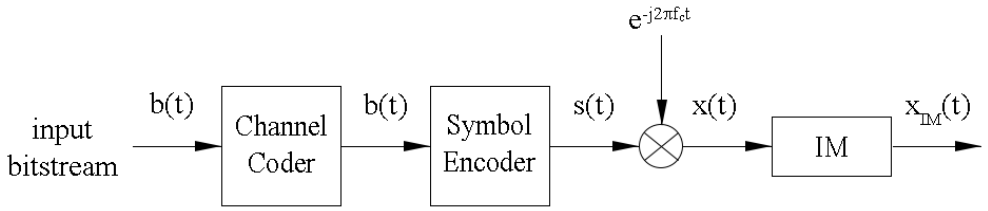


Figure 1: TX component.

## 2.2 Data Configuration

Digital information in the form of bits contains the useful information that needs to be transmitted from the TX of the system to the appropriate receiver. Since the information in it's current form cannot be transmitted, the signal needs to be subjected to various steps in order to become transmittable. These processes have a direct impact on the produced signal's properties, thus rendering them invaluable for a successful communication. Firstly, the digital information $b(t)$, in the form of bits, is subjected to the selected modulation scheme. Modulating a bit-stream has as a result a sequence of complex numbers which are also referred to as symbols. This happens by matching the bit with the appropriate symbol based on the constellation diagram of the modulation. The diagram of each modulation is defined by the alphabet $M$ of the modulation which also impacts the data size transferred and the noise resistance of the signal. The modulation stage completes with the symbol encoder resulting in the symbol signal $s(t)$. In this study, the Binary Phase Shift Keying (BPSK) modulation is used, the constellation diagram of which is presented in Figure 2. BPSK's constellation diagram consists of two symbols placed on the real x axis.

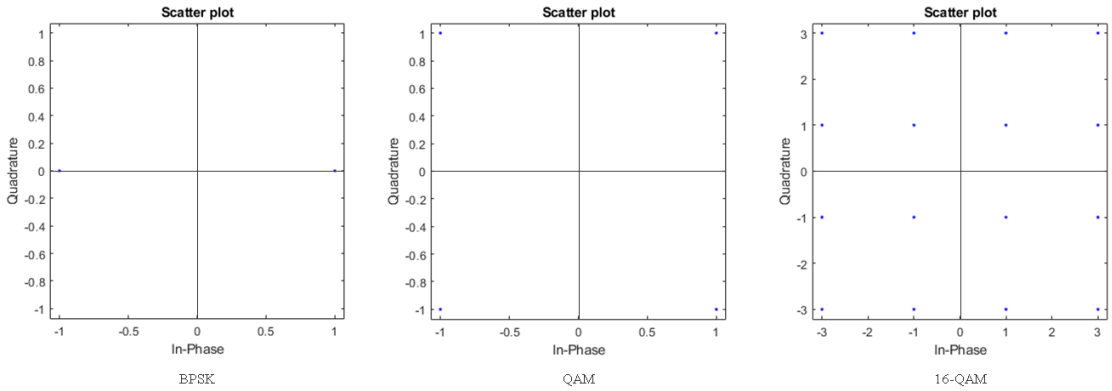


Figure 2: BPSK, QAM and 16-QAM Constellation Diagrams.

## 2.3 Residual Carrier Signal

Alongside with the information signal, TX also transmits a carrier signal $c(t)$. Since attributes such as the amplitude $a$, phase $\phi_c$ and the frequency of the carrier $f_c$ are predetermined, $c(t)$'s value is given for every $t$. The carrier signal is described by the following equation:

$$c(t) = a\sin(2\pi f_c t + \phi_c) \tag{1}$$

Since $c(t)$'s attributes can be predefined, by applying $c(t)$ to the information signal one can bring the latter to a form appropriate for transmission. Based on the modulation scheme, the application of the carrier differs. In BPSK, the information for transmission alters the phase of the carrier $\phi_c$. In this study we apply a non-return to zero (NRZ) BPSK. The equation of the passband signal given by the application of the carrier signal of (1) is:

$$s(t) = a\sin(2\pi f_c t + \phi(t)) \tag{2}$$

With a time variant phase $\phi(t)$. Expanding the sine term in (2) gives:

$$s(t) = a\cos(\phi(t))\sin(2\pi f_c t) + a\sin(\phi(t))\cos(2\pi f_c t) \tag{3}$$

Since we use NRZ BPSK the following are true $cos(\phi(t)) = 1$ and $sin(\phi(t)) = \phi(t)$, thus (3) becomes:

$$s(t) = a\sin(2\pi f_c t) + a\phi(t)\cos(2\pi f_c t) \tag{4}$$

In (4), the sine term describes the carrier signal whereas the cosine term describes the information signal. Using the mixer of Figure 1, we apply $e^{-j2\pi f_c t}$ to (4) and we get the baseband signal $x(t)$:

$$s(t)e^{-j2\pi f_c t} \quad \Rightarrow \quad x(t) = ae^{j\phi(t)} \tag{5}$$

Since the upkeep of information for transmission is not constant, there will be times where TX will not have any useful information to transmit (since we apply Time slot IM these occurrences will be further increased). TX can then choose between either ceasing transmission or transmit trivial information. In this study the latter technique is used by continuing the transmission of the carrier of (1). As a result, $c(t)$ is classified as a residual carrier, whereas in the opposite situation (where no carrier is transmitted) it would have been classified as suppressed.

## 2.4 Index Modulation

Before the signal's transmission, Time slot IM is applied to it at the IM component's stage. During this stage, the transmission times are viewed as time slots which can be classified as activated on whether TX decides to transmit or not. A time slot where a transmission occurs is defined as an active time slot, whereas one where no useful information is transmitted is defined as an inactive time slot. Useful information refers to the contents of the message and not carrier signals. Values can be assigned to the time slots to denote their active status such as a value of "1" for active time slots and "0" for inactive ones. Interpreting the sequence of the active-inactive time slots results in additional information transmitted with benefits such as lower power consumption or bandwidth usage which lead to faster transmission times. Using BPSK with a symbol sequence of [1 -1 -1 1 1 ...], TX can cease transmission for negative values. By using the aforementioned time slot values, a time slot activation sequence of [1 0 0 1 1 ...] occurs. TX will then transmit the "1" valued symbols, otherwise ceasing it's transmission, RX will deduct the "$-1$" valued ones which ultimately reduces the overall power consumption of the transmission scheme. From the above, one can easily deduce that the concept regarding the symbols-time slots sequencing can be modified to transfer additional information by matching the two sequences. An example of such a modification using BPSK, a symbol sequence $s[n] = [1-111-1-11-1...]$ and symbol-to-time slot sequence matching following the previous notation with matches $[-1-1] \rightarrow [00], [-11] \rightarrow [01], [1-1] \rightarrow [10]$ is presented bellow. TX using the matchings as a lookup table will shape it's time slot activation pattern as such:

| i | symbol-to-transfer | following-symbol | ts activation |
|---|---|---|---|
| 1. | [1] | [-1] | [1 0] |
| 2. | [1] | [1] | [1 1] |
| 3. | [-1] | [-1] | [0 0] |
| 4. | [1] | [-1] | [1 0] |
| 5. | ... | ... | ... |

Table 1: Table of symbol-to-time slot sequence matching.

The produced activation sequence is given by the *ts activation* column and is equal to [10110010...].

| i | ts activation | transferred symbol(s) | received symbols | deducted symbols |
|---|---|---|---|---|
| 1. | [1 0] | [1] | [1] | [-1] |
| 2. | [1 1] | [1 1] | [1 1] | – |
| 3. | [0 0] | – | – | [-1 -1] |
| 4. | [1 0] | [1] | [1 ] | [-1] |
| 5. | ... | ... | ... | ... |

Table 2: TX-RX communication with Time slot IM.

From the previous example it is shown that it is possible to further increase the additional information encoded in the activation patterns by increasing the group size of the time slots. Instead, in this study, we focus on the overall effect that the Time slot IM has on the transmission noise and error wise, thus no further study is done on these parts. The central idea of the study is shown in Figure 3:

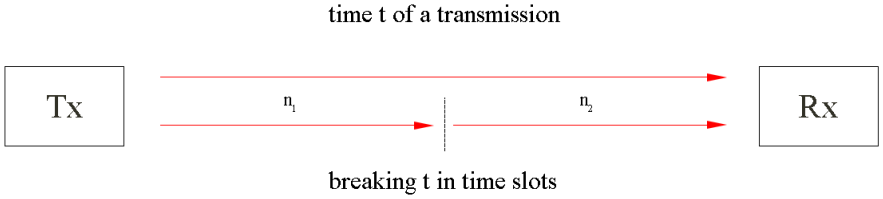


Figure 3: Transmission with Time slot IM.

# CHAPTER 3: COMMUNICATION CHANNEL

At this point $x_IM(t)$ is transmitted in the form of electromagnetic energy. The medium in which the transmission takes place is characterized as a communication channel shown in Figure 4. The channel in the form of a filter attenuates $x_{IM}(t)$ producing the signal $y(t)$. Since the study uses the natural environment as the communication channel, the signal passing through it has it's values altered due to the channel's impulse response, as well as the various processes taking place in the environment.

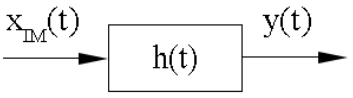


Figure 4: Transmission channel between TX and RX.

## 3.1 Modelling the Channel as a Filter

The communication channel is modeled as a filter $h(t)$ through which the signal passes. The transfer function of the filter, $H(f)$, provides it's impulse response (IR) $h$. Applying it to $x_{IM}(t)$, the resulted signal is given by the convolution of the two:

$$x'_{IM}(t) = h(t) * x_{IM}(t) \tag{6}$$

where

$$h(t) * x_{IM}(t) = \int_{-\infty}^{\infty} h(\tau) x_{IM}(t-\tau) d\tau$$

The components dictating the nature of the environment shape it's mathematic model. The physical distance between TX and RX results in a delay between transmission and reception called propagation delay. The electromagnetic energy that bounces off in surfaces existing in the transmission's environment cause additional signals to be received by RX leading to Intersymbol Interference (ISI) explained in Figure 5:

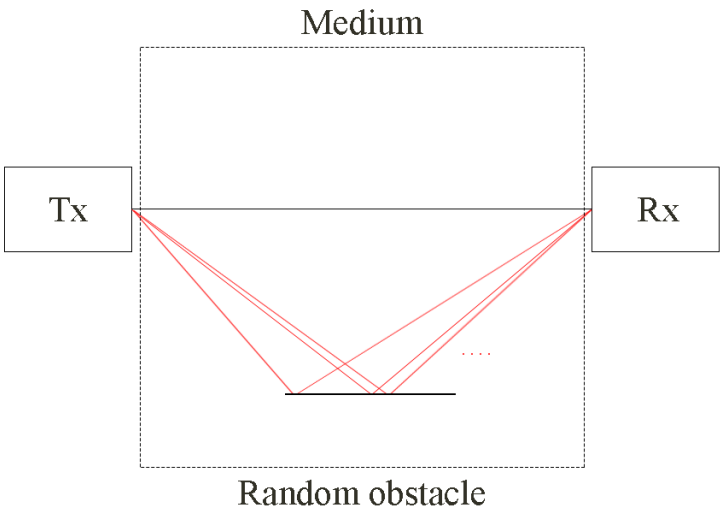


Figure 5: ISI.

Additional to the Line of Sight (LOS) displayed as a black line which shows the direct path between TX-RX, multiple signals are being received due to the initial signal bouncing off surfaces of the environment. These additional signals have altered attributes and are described in (7):

$$h(t) = \sum_i a_i \cos(2\pi f_c t + \phi_i(t)) \tag{7}$$

with $i = 1, 2, ...$ the multiple instances of the signals, $a_i$ the altered amplitude of each signal and $phi_i(t)$ their phase. Expanding the cosine term in (7) we get:

$$\begin{aligned}(7) &= \sum_i [a_i \cos(\phi_i(t)) \cos(2\pi f_c t)] - \sum_i [a_i \sin(\phi_i(t)) \sin(2\pi f_c t)] \\ &= \sum_i a_i \cos(\phi_i(t)) \cos(2\pi f_c t) - \sum_i a_i \sin(\phi_i(t)) \sin(2\pi f_c t) \\ &= r_i(t) \cos(2\pi f_c t) - r_q(t) \sin(2\pi f_c t) \end{aligned} \tag{8}$$

where $r_i(t)$ and $r_q(t)$ are the sums of random variables with equal PDFs. Using the Central Limit Theorem (CLT), $r_i(t)$ and $r_q(t)$ are Gaussian random variables:

$$h(t) = r_i(t) + j r_q(t) \tag{9}$$

Since $h(t)$ is a complex number, by converting it to it's polar coordinates we receive the following form:

$$h(\theta) = |h| \angle \theta, \quad where \quad \theta = \tan^{-1}\left(\frac{r_q}{r_i}\right) \tag{10}$$

Using (6) we can apply the channel's $h(t)$ to a symbol $x = a + jb \Rightarrow x = |x|\angle\phi$ resulting to the filtered version of the symbol:

$$x' = h_1 x = |h_1||x|\angle(\theta_1 + \phi) \tag{11}$$

From (11) it is now obvious how the channel alters the signal through the application of $h$ on the symbols. Due to the channel being the natural environment the following holds $|h| < 1$. This reduces the filtered symbol's amplitude and can be perceived as a reduction to the vector's magnitude. Secondly, IR's phase alters the phase of the symbol, which translates to a rotation of the symbol.

### 3.2 Additive White Gaussian Noise

Another aspect of the channel that further affects the signal's transmission is the noise that exists in said channel. Noise is the result of multiple other processes happening in the same environment as the transmission. There is a plethora of mathematical models for noise simulation, but in this study the Additive White Gaussian Noise (AWGN) model is followed. AWGN has $PSD = N_0$ $Watt/Hz$, is added to the signal and follows a normal distribution with zero mean value. Taking the above into account, (6) becomes:

$$y(t) = x'_{IM}(t) + n(t) = h(t) * x_{IM}(t) + n(t) \tag{12}$$

Where $n(t)$ is the AWGN function, and the channel of Figure 4 is now further analysed into Figure 6.

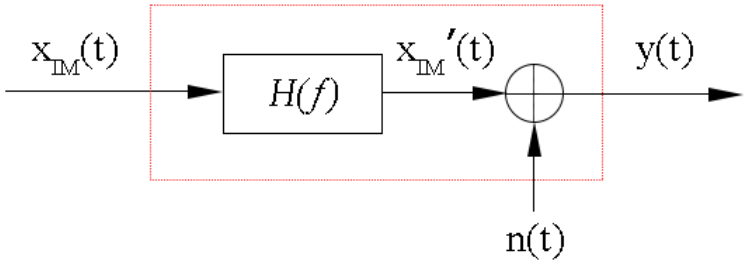


Figure 6: Channel analysis.

At this point, the symbols received by RX will have the following form:

$$y_1 = x' + n_1 = h_1 x + n_1 = |h_1||x|\angle(\theta_1 + \phi) + n_1$$

In the value of the already rotated and with reduced amplitude symbols, the value of the noise signal is added contributing to even higher attenuation. All of the above show the importance of the channel's state and how it affects the transmitted signal as it directly impacts the number of errors in it's reception.

# CHAPTER 4: RECEIVER

## 4.1 Data Reception

Due to the factors described in Chapter 3, RX must submit the received signal to certain stages to undo the attenuation affecting it. RX follows the stages pictured in Figure 7.

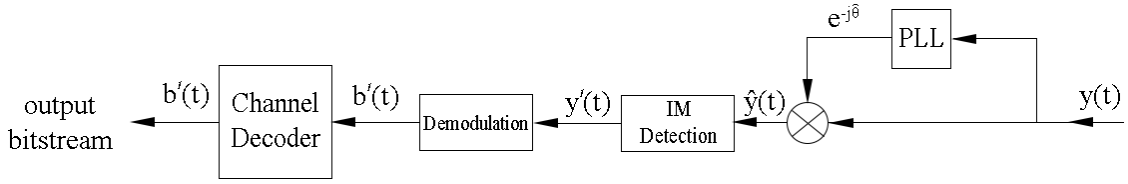


Figure 7: RX component.

## 4.2 Phase Detection

In order to undo the changes made to the signal, we must further analyse the way it is affected by the channel. The discreet representation of (12) is:

$$y[n] = h[n] * x_{IM}[n] + n[n]$$

By viewing $y[n]$ as a vector equal to the multiplication of the table $H$, containing the channel's taps, with the vector $x_{IM}$, containing the values of $x_{IM}[n]$ for every $n$, adding the noise vector $n$ we get the equation:

$$y = Hx_{IM} + n \tag{13}$$

Since a SISO approach is used in this study, the IR will have a singular tap value throughout the communication, thus $H$ is a vector $h$, (13) then becomes:

$$y = hx_{IM} + n \tag{14}$$

where undoing $h$ is described as:

$$\hat{y} = \frac{1}{|h|}\angle(y_{angle} - \theta) \tag{15}$$

From (14) and (15), it is obvious that undoing the effects of the channel's IR is equal to undoing the amplitude and phase of $h$. Due to the complexity of calculating an approximation for the IR's amplitude, we focus on the calculation of $h$'s phase. This is achieved by using a Phase-Locked Loop component at the RX's reception.

## 4.3 Phase-Locked Loop

The Phase-Locked Loop (PLL) is described in Figure 8, where the received signal enters the first stage of the PLL. The approximation of the IR's phase $\widehat{\theta}(t)$ is achieved using the differentiations in $y(t)$'s values.

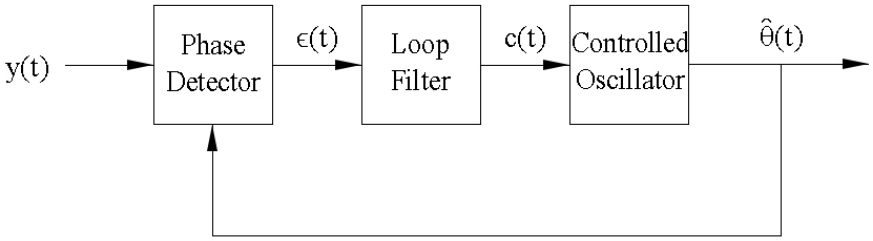


Figure 8: Stages of a PLL.

### 4.3.1 Phase Detector

In this stage, an approximation error $\epsilon(t)$ of the channel's phase is calculated during each iteration using $y(t)$'s phase $\theta(t)$ and the channel's phase approximation of the previous iteration $\hat{\theta}(t)$. The error is equal to $\epsilon(t) = \theta(t) - \hat{\theta}(t)$ and thus $\epsilon(t) \to 0 \Rightarrow \hat{\theta}(t) \to \theta(t)$, resulting in a better approximation.

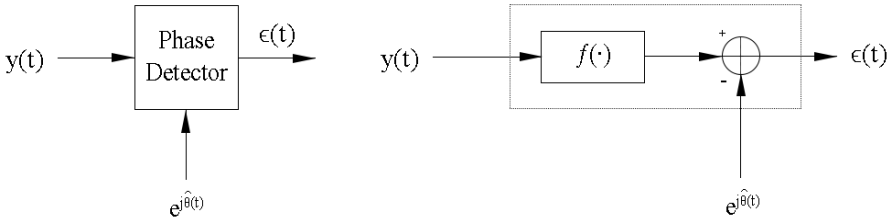


Figure 9: Phase Detector.

As shown in Figure 9, the passband signal $y(t)$ can be described as $e^{j\theta} + n(t)$, where $e^{j\theta}$ is the phase of the information $\phi$ signal altered from the channel's ir. Since the phase of the symbols is predetermined by the modulation scheme used, using the Adder component of the phase detector, we can omit $\phi$ and thus isolate $\hat{\theta}$. Eradicating the symbol's phase is achieved by taking advantage of the correlation between each symbol's phase. In BPSK, as shown in Figure 2, since the two symbols comprising the constellation diagram have phase equal to 0 or $\pi$, the correlation between the two is $\pi$ rads, which leads to:

$$\theta_{pi} = \theta_0 + \pi$$
$$2\theta_{pi} = 2\theta_0 + 2\pi$$
$$\sin(2\theta_{pi}) = \sin(2\theta_0 + 2\pi) = \sin(2\theta_0)$$

The symbol phase convergence described above is schematically explained in Figure 10 where a singular tap $h$ equal to $-\frac{\pi}{6}$ was used and it can be similarly applied for any phase:

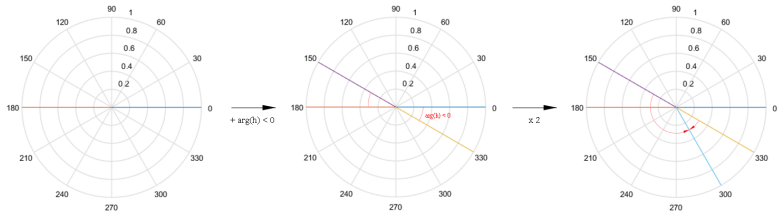

Figure 10: BPSK symbol phase convergence.

Furthermore, multiplying the symbol's phase by 2 leads to their convergence to a singular value, which then can be redacted without the explicit knowledge of it's value. For this to hold true, they need to converge to a positive quadrant for the correct approximation of $h$. The value chosen for the multiplication of the phase is inseparably linked with the modulation scheme applied and it's alphabet. Based on the alphabet of the modulation the same value of multiplications need to be made. As an example, symbol phase convergence for QAM is shown in Figure 11:

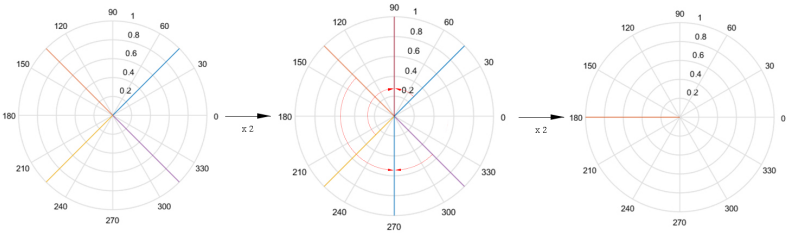

Figure 11: QAM symbol phase convergence.

Since the phase converged in a negative quadrant, appropriate actions need to be made for a correct result. These are explained in Chapter 5 and are described schematically as the $f$ component of the phase detector in Figure 9.

### 4.3.2 Loop Filter

After calculating the error, this enters the loop filter stage. The basic attributes of the loop filter $L(s)$ are defined in this stage. Depending on $L(s)$ we have:

$$L(s) = K_L = constant$$

The PLL is classified as a first order PLL, with transfer function:

$$H(s) = \frac{K_L}{K_L + s}$$

The simplicity of the first order PLL renders it susceptible to noise since it has no component for filtering it. If the loop filter is described by the following function:

$$L(s) = K_L \frac{a+s}{b+s} \tag{16}$$

The PLL is classified as a second order PLL. Setting $b = 0$ results in:

$$L(s) = K_L \frac{a+s}{s} = K_L + K_L \frac{a}{s} \tag{17}$$

Making it a PI (proportional-integral) loop filter as it is comprised of an integrator proportional to the input $K_p$ and an integrator proportional to the integral of the input $K_i$. The transfer function of a second order PI PLL is equal to:

$$H(s) = \frac{K_L a + K_L s}{K_L a + K_L s + s^2} \tag{18}$$

The first parameter that we will analyse, is the damping factor $\zeta$ of the PLL:

$$\zeta = \frac{1}{2}\sqrt{\frac{K_L}{a}} \tag{19}$$

$\zeta$ defines the range of values of the approximation $\hat{\theta}(t)$ until it converges. Depending on $\zeta$ the following cases occur:

- $\zeta < 1$ the system is underdamped, showing a wide range of values for $\hat{\theta}(t)$
- $\zeta = 1$ the system is critically damped, offering a tighter range of values
- $\zeta > 1$ the system is overdamped, offering the tightest range of values

The next parameter is the natural frequency $w_n$ of the PLL:

$$w_n = \sqrt{K_L a} \tag{20}$$

$w_n$ affects the loop bandwidth of the PLL and more specifically the noise bandwidth $B_L$ which comprises the PLL's low-pass filter:

$$B_L = \frac{w_n}{2}\left(\zeta + \frac{1}{4\zeta}\right) \tag{21}$$

Selecting the appropriate $B_L$ value differs in each application since the following trade-off occurs. A small noise bandwidth value leads to more noise filtered which also leads to filtering frequencies useful for the phase approximation thus converging to a value slower compared to a PLL with a bigger $B_L$ value. In addition, a bigger bandwidth value leads to a noisy phase approximation. Due to the importance of the noise bandwidth value to the PLL's efficiency, we give an appropriate value to $B_L$ first and then to $\zeta$ and $w_n$ as they are directly correlated to it's value. From (19), (20), (21) a second order PLL (which is also used in this study) has a transfer function of:

$$H(s) = \frac{w_n^2 + 2\zeta w_n s}{w_n^2 + 2\zeta w_n s + s^2} \tag{22}$$

(22) shows how the aforementioned parameters directly define the PLL's operation. Also, $K_i$ and $K_p$ directly affect the loop filter, since:

- *(proportional)* $K_p = 2\zeta w_n T_s$, where $T_s$ the sampling frequency
- *(integral)* $K_i = w_n^2 T_s^2$

After the stage of the loop filter, $\epsilon(t)$, produces a control signal $c(t)$ which is then used in the stage of the Voltage Controlled Oscillator.

### 4.3.3 Voltage Controlled Oscillator

The final stage of the PLL consists of a voltage controlled oscillator (VCO) whose phase can be altered based on the input signal. VCO's input is the control signal $c(t)$ calculated in the previous stage; depending on $c(t)$'s amplitude, VCO's phase is altered accordingly. The control signal alongside with the angular frequency of the VCO are used to calculate $\widehat{\theta}$:

$$\begin{aligned} w &= \frac{d(2\pi f_c t + \widehat{\theta}(t))}{dt} \\ &= 2\pi f_c + \frac{d\widehat{\theta}(t)}{dt} \end{aligned}$$

with $\frac{d\widehat{\theta}(t)}{dt} = c(t)$:

$$w = 2\pi f_c + c(t), \quad \widehat{\theta}(t) = \int_{-\infty}^{t} c(\tau) d\tau$$

## 4.4 Index Modulation

At this stage, the RX must identify the nature of the time slot when the reception was made, meaning the classification between an active and an inactive time slot. Due to the transmission taking place in a natural environment, time slots where no transmission from the TX is made, will still contain information due to the noise of the channel as explained previously. Thus we devise the stage of IM Detection, where based on the signal's power, it is identified as noise and discarded or as useful information which then proceeds on to the stage of symbol demodulation. Simultaneously, the additional information from the active states of the time slots is matched to the correct values.

# CHAPTER 5: TOPOLOGY

The overall communication model described in the previous chapters is displayed in Figure 12. For the communication between TX and RX a carrier signal is used forming the complex passband signal $x(t)$ to which Time slot IM is applied. The transmitted signal is filtered by the channel's impulse response leading to the received attenuated signal $y(t)$. By identifying the IR's phase $\hat{\theta}$ and the sequence of the active-inactive sequence of the time slots, we get the output bitstream $b'(t)$.

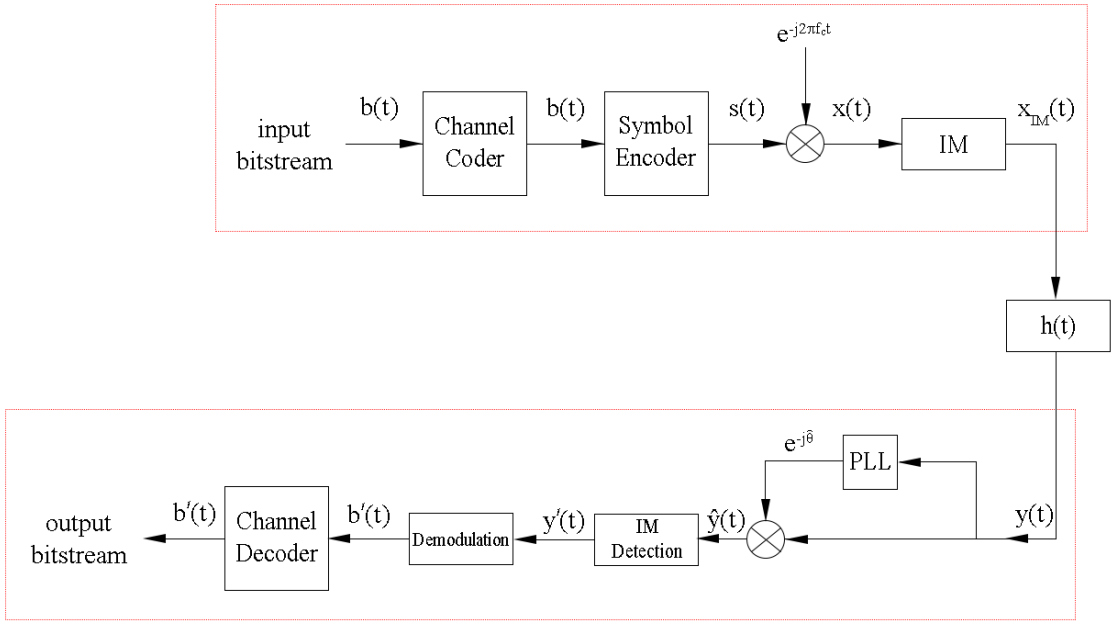


Figure 12: The system's complete topology.

At this point, the topology followed in this study as well as the theoretical background for each component's function has been fully analysed. The algorithms describing the system's components used in this study are analysed bellow.

## 5.1 TX Implementation

Algorithm 1 describes the TX component of the communication system. TX produces the symbol stream $s$, the carrier signal $c$ as well as the activation sequence of the time slots contained in $x_{IM}$ alongside with the symbols to be transmitted.

**Algorithm 1:** Tx component

**Input:** Sample rate $\rightarrow T$
**Input:** Bit signal sampled at $t = nT \rightarrow b$
**Input:** Carrier amplitude, phase $\rightarrow a, \phi$
**Input:** Modulation Alphabet $\rightarrow M$
**Output:** $x_{IM}, carrier$
$s = BPSKModulation(b, M)$;
$x_{IM} = TimeSlotIndexModulation(s)$;
$SizeOf(carrier) = SizeOf(x_{IM})$;
$carrier = a$ ; `// vector containing the scalar value` $a$, $SizeOf(carrier)$ `- times`

The implementation of Time slot Index Modulation in TX is shown in algorithm 2. The additional information transferred during Time slot IM is based on the sequence of the time slots' activation states. In this study, we focus on a *random* sequence scheme decided by TX so as to study the complete behavior of the scheme. The number of time slots forming each group is 2, thus $2^2$ cases. Following the notation presented in Chapter 1.4 the time slot cases available are [00 01 10 11].

**Algorithm 2:** Time slot IM in TX

**Input:** Baseband signal $\rightarrow x$
**Output:** Transmission signal including time slots $\rightarrow x_{IM}$
$k, i = 1$;
**while** *true* **do**
    $case = Pick([00 \quad 01 \quad 10 \quad 11])$ ;  `// Pick function returns a random element from vector argument`
    **if** $case = 00$ **then**
        $x_{IM_k} = 0$;
        $x_{IM_{k+1}} = 0$;
        $k = k + 2$;
    **else if** $case = 01$ **then**
        $x_{IM_k} = 0$;
        $x_{IM_{k+1}} = x_i$;
        $k = k + 2$;
        $i = i + 1$;
    **else if** $case = 10$ **then**
        $x_{IM_k} = x_i$;
        $i = i + 1$;
        $x_{IM_{k+1}} = 0$;
        $k = k + 2$;
    **else**
        $x_{IM_k} = x_i$;
        $i = i + 1$;
        **if** $i >= SizeOf(s)$ **then**
            $x_{IM_{k+1}} = 0$ ;  `// if no other element for second time slot, send an inactive one`
        **else**
            $x_{IM_{k+1}} = x_i$;
            $i = i + 1$;
        **end**
        $k = k + 2$;
    **if** $i > SizeOf(x)$ **then**
        b
    **else**
        r
    **end**
    eak;
**end**

The values of $x_{IM}$ will be equal to 0 for inactive time slots and equal to the corresponding symbol value of the BPSK modulation for active time slots both of which values are tampered with as the signal is filtered through the channel.

## 5.2 Communication Channel Implementation

The communication channel algorithm is described in chapters 6.1 and 6.2 where the difference between the AWGN and Rician fading channel is analysed.

## 5.3 RX implementation

RX's basic function is described in algorithm 3.

**Algorithm 3:** Rx component

**Input:** PLL parameters $\rightarrow B_L, w_n, \zeta$
**Input:** PLL sampling rate $\rightarrow T_s$
**Input:** Distorted symbol signal in Rx input $\rightarrow y$
**Input:** Modulation alphabet $\rightarrow M$
**Output:** Output bit-stream $\rightarrow b'$
$\hat{\theta} = PLL(B_L, w_n, \zeta, y)$ ; `// ` $\hat{\theta}$ `is the approximation of the channel's ir phase`
$\hat{y} = ye^{-j\hat{\theta}}$;
$y' = TimeSlotIndexDemodulation(\hat{y})$;
$b' = BPSKDemodulation(y', M)$;

The following algorithm comprises the PLL stage of the RX. The stage of the phase detector, loop filter and VCO are separate functions part of algorithm 4. The resulting phase approximation $\hat{\theta}$ is then used for negating the IR's phase.

**Algorithm 4:** PLL

**Input:** Distorted symbol signal in Rx input $\rightarrow y$
**Input:** PLL parameters $\rightarrow B_L, w_n, \zeta, T_s$
**Output:** IR's phase approximation vector $\rightarrow \hat{\theta}$
$n = 2$;
$integrator = 0$;
$SizeOf(\hat{\theta}) = SizeOf(y)$;
$\hat{\theta} = 0$ ; `// a vector containing the scalar value of 0,` $SizeOf(\hat{\theta})$ `- times`
$SizeOf(c) = SizeOf(y)$;
$c = 0$ ; `// control signal` $c(t)$
$w_n = \frac{2B_L}{\zeta + \frac{1}{4\zeta}}$;
$K_i = w_n^2 T_s^2$;
$K_p = 2\zeta w_n T_s$;
**while** $n <= SizeOf(y)$ **do**
  $\epsilon_n = PhaseDetector(\hat{\theta}_{n-1}, carrier)$;
  $integrator = integrator + K_i \epsilon_n$;
  $proportional = K_p \epsilon_n$;
  $c_n = proportional + integrator$;
  $\theta_n = PhaseApproximation(\hat{\theta}_{n-1}, c_{n-1})$;
**end**

Algorithm 5 describes the phase detector of Chapter 4.3.1. It also shows the importance of a positive sine value, as well as the suppression of the symbol's phase.

**Algorithm 5:** Phase Detector

**Input:** Received signal $\rightarrow y$
**Input:** IR's phase approximation from previous iteration $\rightarrow \widehat{\theta}$
**Input:** Modulation alphabet $\rightarrow M$
**Output:** Phase error $\rightarrow \epsilon$
$diff = angle(y) - \widehat{\theta}$;
$\epsilon = \sin(-sign(j^M) \cdot M \cdot diff)$ ; `// where` $M$ `is the modulation's alphabet`

By taking advantage of the carrier signal transmitted continuously by the TX even in inactive time slots, we can further modify (5) resulting in a more accurate calculation of the error $\epsilon$. In (4), we can discern the term corresponding to the carrier signal from the term containing the information signal and regardless of it's conversion to a passband signal, this variation still stands. The carrier term shows smaller variations in it's values as opposed to the fast changing data term. Thus by focusing on the carrier term we get better approximations regarding their accuracy. Applying all of the above, we get:

**Algorithm 6:** Phase Detector

**Input:** Carrier signal $\rightarrow carrier$
**Input:** IR's phase approximation from previous iteration $\rightarrow \widehat{\theta}$
**Output:** Phase error $\rightarrow \epsilon$
$\epsilon = angle(y) - \widehat{\theta}$;

The PLL's VCO of Chapter 4.3.3 is outlined in algorithm 7:

**Algorithm 7:** Phase Approximation.

**Input:** IR's phase approximation scalar $\rightarrow \theta_{n-1}$
**Input:** Control signal scalar $\rightarrow c_{n-1}$
**Output:** IR's phase approximation scalar $\rightarrow \theta_n$
$\theta_n = \theta_{n-1} + c_{n-1}$;
**if** $abs(\theta_n) > \pi$ **then**
  $\theta_n = \theta_n - 2\pi sign(\theta_n)$;
**end**

Parallel to the approximation of the channel's phase, the input signal enters the stage of Time slot Index Demodulation. The resulting $y'$ is free of inactive time slots and contains only the symbols transferred during the active time slots:

**Algorithm 8:** Time slot Index Demodulator.

**Input:** IM signal $\rightarrow y$
**Input:** Noise threshold $\rightarrow n_T$
**Output:** Index demodulated signal $\rightarrow y'$
$i, j = 1$;
**while** $i <= SizeOf(y)$ **do**
    **if** $norm(y_i) - n_T > 0$ **then**
        $y'_j = y_i$;
        $j = j + 1$;
    **end**
    $i = i + 1$;
**end**
`// in this scope a helper vector can be introduced to assist in Bit Error Rate calculation`

Time slot Index Demodulator utilizes the Euclidean norm of each data $y_i$ to classify it as noise or symbol. At this point we also calculate the Bit Error Rate (BER) of the transmission. BER is defined as:

$$BER = \frac{number\_of\_wrong\_bits}{number\_of\_total\_transmitted\_bits} \tag{23}$$

In Time slot IM, BER is modified to take into account the miss-classification of the active-inactive time slots due to noise. BER calculation in this case, focuses on:

- The correct categorisation of the time slots/symbols.
- The number of wrong bits from BPSK demodulation.
- Addition of the above and division of the result with the sum of the time slots and the bits at the exit $b'$.

Thus (23) becomes:

$$BER = \frac{number\_of\_wrong\_time\_slot\_classification + number\_of\_wrong\_bits}{number\_of\_total\_transmitted\_time\_slots + number\_of\_bits\_at\_output}$$

The above procedure respects the order of the bits, in this way they are compared with their appropriate counterparts.

# CHAPTER 6: RESULTS

The algorithms presented above where coded in the Matlab© environment of Mathworks© and the results are displayed bellow. Two cases where studied, one where the channel is described as an AWGN only channel and thus it's impulse response has a singular value, constant for the duration of the transmission. In the second one a rician channel is used where the $LOS$ effects mentioned in Chapter 3.1 are applied, meaning the value of $h$ is changing based on the signal's power and the channel's characteristics. For each case, different values of $SNR$ and $CNR$ where used. Studying the behavior of the system based on the $CNR$ was deemed appropriate since it is directly used for the phase approximation. The values $CNR = 0, 10, 20dB$ where used and for each case $SNR$ received values of $-5, 0, 5, 10dB$. The resulting BER is then compared to the BER of the transmission without the application of Time slot IM, as well as a comparison between the throughputs of the two schemes is made. Additionally, the throughput of Time slot IM is governed by the fact that 1-bit additional information can be transmitted due to the time slot sequencing.

## 6.1 Results for AWGN Channel

Algorithm 9 describes the steps taken for the simulation of the AWGN channel and it's effects on the transmitted signal:

**Algorithm 9:** AWGN channel.

**Input:** Time slot IM signal $\rightarrow x_{IM}$
**Input:** Carrier signal $\rightarrow c$
**Input:** Signal-to-Noise and Carrier-to-Noise ratios $\rightarrow SNR, CNR$
**Output:** Distorted symbol, carrier signal $\rightarrow y, c'$
Set $h_0$ ; `// The one-tap` $h$ `value of the channel's impulse response in polar form e.g.` $h_0 = 1\angle 0$
$y = h_0 \cdot x_{IM}$;
$c' = h_0 \cdot c$;
Create AWGN channel $n_1$; `// Creation of` $n(t)$ `as presented in Section 3.2 based on SNR. Function comm.AWGNChannel© of Matlab© was used, with arguments ('NoiseMethod', 'Signal to noise ratio (SNR)', 'SNR', SNR.`
$y = n_1(y)$ ; `// Applying AWGN to symbols` $y = h_0 \cdot x_{IM} + n_1$.
Create AWGN channel $n_2$; `// Creation of` $n(t)$ `as presented in Section 3.2 based on CNR. Function comm.AWGNChannel© of Matlab© was used, with arguments ('NoiseMethod', 'Signal to noise ratio (SNR)', 'SNR', CNR.`
$c' = n_2(c)$ ; `// Applying AWGN to carrier` $c' = h_0 \cdot c + n_2$.

In Figure 13, we can observe that the BER of Time slot IM follows a slower pace of reduction compared to it's counterpart, where no IM schemes are applied. This is due to the fact that errors can occur in the identification of the time slots.

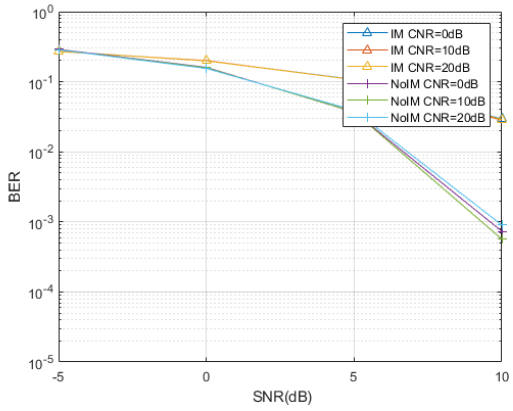


Figure 13: BER of time slot IM versus no-IM for AWGN channel..

The throughput comparison in Figure 14, confirms that Time slot IM outweigh it's counterpart due to the additional information that is mentioned throughout the study.

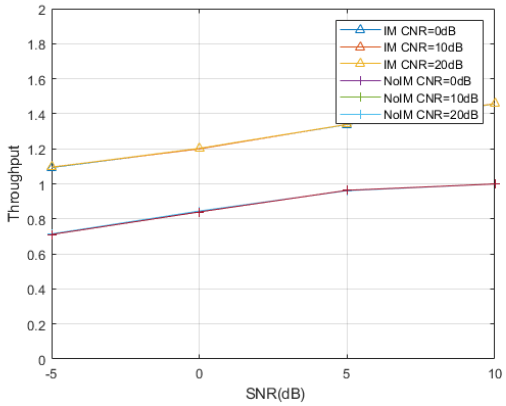


Figure 14: Throughput of time slot IM versus no-IM for AWGN channel.

Last but not least, in Figure 15, the approximation of $\hat{\theta}$ is displayed. In this particular simulation, $h = 1\angle 0$ throughout the transmission. $CNR$ also directly affects the quality of the approximation

(cases of $0dB$ and $10dB$) as hypothesised previously, where it converges after a certain value (cases of $10dB$ and $20dB$).

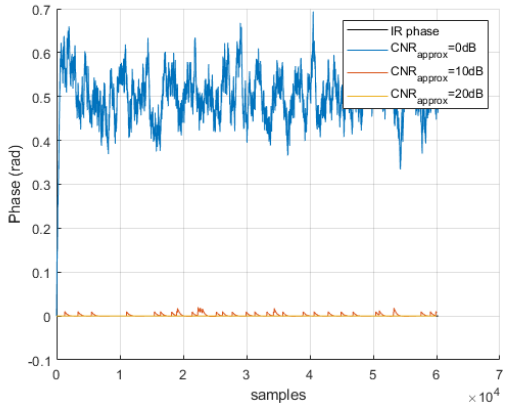


Figure 15: Phase approximation for AWGN channel.

## 6.2 Results for Rician Channel

Algorithm 10 describes the steps taken for the simulation of the rician channel and it's effects on the transmitted signal with notable differences with Algorithm 9:

**Algorithm 10:** Rician channel.

**Input:** Time slot IM signal $\rightarrow x_{IM}$
**Input:** Carrier signal $\rightarrow c$
**Input:** Signal-to-Noise and Carrier-to-Noise ratios $\rightarrow SNR, CNR$
**Output:** Distorted symbol, carrier signal $\rightarrow y, c'$
Set $h$ ; `// Creation of impulse response of Rician channel using ricianchan © of Matlab© with sample time of the input signal equal to that of the PLL` $ts = Ts$, `maximum Doppler shift equal to 1` $fd = 1$, `Rician K-factor equal to 1` $k = 1$.
$y = filter(h, x_{IM})$;
$c' = filter(h, c)$;
Create AWGN channel $n_1$; `// As presented in Algorithm 9.`
$y = n_1(y)$ ; `// Applying AWGN to symbols` $y = h. \cdot x_{IM} + n_1$.
Create AWGN channel $n_2$; `// As presented in Algorithm 9.`
$c' = n_2(c)$ ; `// Applying AWGN to carrier` $c' = h. \cdot c + n_2$.

In Figure 16, we can observe that the BER of Time slot IM follows a slower pace of reduction compared to it's counterpart, where no IM schemes are applied. This is due to the fact that errors can occur in the identification of the time slots, similar with Figure 13.

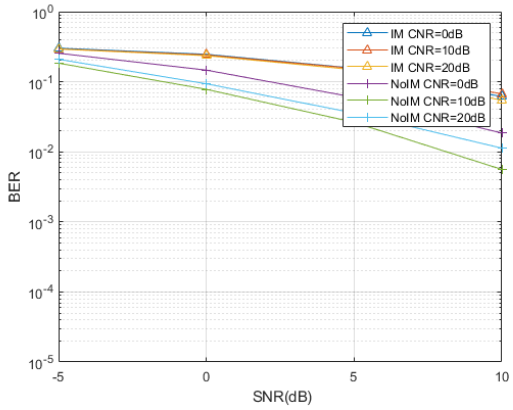


Figure 16: BER of time slot IM versus no-IM for Rician channel.

As in the AWGN case, the throughput comparison in Figure 17, again confirms that Time slot IM outweighs it's counterpart due to the additional information transmitted.

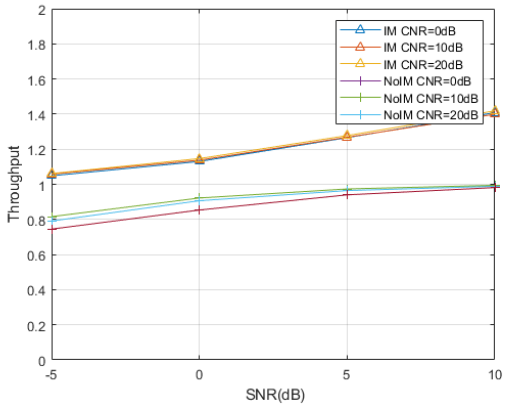


Figure 17: Throughput of time slot IM versus no-IM for Rician channel.

In the case of the rician channel, one can better understand the accuracy of the PLL in calculating the approximation of the IR's phase. In Figure 18, the approximation of $\hat{\theta}$ is displayed. In this particular simulation, $h = 1\angle 0$ throughout the transmission. $CNR$ also directly affects the quality of the approximation (cases of $0dB$ and $10dB$) as hypothesised previously, where it converges after a certain value (cases of $10dB$ and $20dB$).

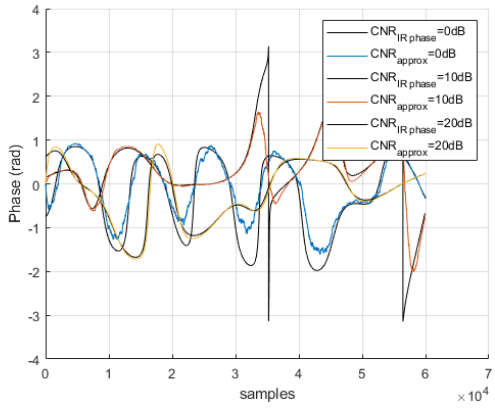


Figure 18: Phase approximation for Rician channel.

# CHAPTER 7: CONCLUSION

In this study, the Time slot IM scheme was applied in a SISO system of wireless communication between TX-RX with a BPSK modulation scheme. The SISO topology lead to the channel's impulse response to be consisted of a singular tap. The channel's attenuation on the transmitted signal was negated using a second order PI PLL at the RX, as well as the identification of the active and inactive time slots by the RX.
Taking into account the complete topology as well as the codependancies between the functionalities of the system, we can discern the critical points which can optimize it's efficiency. The trade-off mentioned in Chapter 4.3.2 regarding the noise bandwidth of the PLL, the reduced BER of the Time slot IM which leads to lower throughput as well as the effect of the modulation used in the application, directly affect the performance of the system's components. Due to the different alphabet of each modulation scheme, the robustness of the transmitted signal varies in each application, thus research is required for the effects between different types of modulations (QPSK, QAM, etc.) have in combination with Time slot IM. Moreover, the study of Time slot IM can be further expanded in multi-channel systems and MIMO topologies and how transmissions from different antennas affect each other's time slot sequencing.

# BIBLIOGRAPHY


[1] R. Zeqiri, F. Idrizi, and H. Halimi, "Comparison of Algorithms and Technologies 2G, 3G, 4G and 5G," in *2019 3rd International Symposium on Multidisciplinary Studies and Innovative Technologies (ISMSIT)*, 2019, pp. 1–4.

[2] L. Chettri and R. Bera, "A Comprehensive Survey on Internet of Things (IoT) Toward 5G Wireless Systems," *IEEE Internet of Things Journal*, vol. 7, no. 1, pp. 16–32, 2020.

[3] I. T. Union, "SERIES Y: GLOBAL INFORMATION INFRASTRUCTURE, INTERNET PROTOCOL ASPECTS AND NEXT-GENERATION NETWORKS Next Generation Networks – Frameworks and functional architecture models," United Nations patentus Y.2060, 2012. [Online]. Available: https://www.itu.int/rec/T-REC-Y.2060-201206-I/en

[4] R. Jonathan, S. Douglas C., and B. Lisa, *Fundamental Principles of Optical Lithography*. Wiley, 2015.

[5] R. I. Ansari, H. Pervaiz, S. A. Hassan, C. Chrysostomou, M. A. Imran, S. Mumtaz, and R. Tafazolli, "A New Dimension to Spectrum Management in IoT Empowered 5G Networks," *IEEE Network*, vol. 33, no. 4, pp. 186–193, 2019.

[6] A. A. Purwita, A. Yesilkaya, T. Cogalan, M. Safari, and H. Haas, "Generalized Time Slot Index Modulation for LiFi," in *2019 IEEE 30th Annual International Symposium on Personal, Indoor and Mobile Radio Communications (PIMRC)*, 2019, pp. 1–7.

[7] P. Banelli, S. Buzzi, G. Colavolpe, A. Modenini, F. Rusek, and A. Ugolini, "Modulation Formats and Waveforms for 5G Networks: Who Will Be the Heir of OFDM?: An overview of alternative modulation schemes for improved spectral efficiency," *IEEE Signal Processing Magazine*, vol. 31, no. 6, pp. 80–93, 2014.

[8] E. Memisoglu, E. Basar, and H. Arslan, "Fading-aligned OFDM with index modulation for mMTC services," *Physical Communication*, vol. 35, 2019.

[9] E. Basar, "Reconfigurable Intelligent Surface-Based Index Modulation: A New Beyond MIMO Paradigm for 6G," *IEEE Transactions on Communications*, vol. 68, no. 5, pp. 3187–3196, 2020.

[10] E. Basar, M. Wen, R. Mesleh, M. Di Renzo, Y. Xiao, and H. Haas, "Index Modulation Techniques for Next-Generation Wireless Networks," *IEEE Access*, vol. 5, pp. 16 693–16 746, 2017.

[11] M. Hanif and H. H. Nguyen, "Non-Coherent Index Modulation in Rayleigh Fading Channels," *IEEE Communications Letters*, vol. 23, no. 7, pp. 1153–1156, 2019.

[12] M. Nakao, T. Ishihara, and S. Sugiura, "Single-Carrier Frequency-Domain Equalization With Index Modulation," *IEEE Communications Letters*, vol. 21, no. 2, pp. 298–301, 2017.

[13] S. Jacob, N. T. Lakshmi, and A. Chockalingam, "Dual-Mode Index Modulation Schemes for CPSC-MIMO Systems," in *2018 IEEE 88th Vehicular Technology Conference (VTC-Fall)*, 2018, pp. 1–5.

[14] M. Wen, X. Cheng, M. Ma, B. Jiao, and H. V. Poor, "On the Achievable Rate of OFDM With Index Modulation," *IEEE Transactions on Signal Processing*, vol. 64, no. 8, pp. 1919–1932, 2016.

[15] D. Slepian, "permutation modulation," *Proceedings of the IEEE*.

[16] G. Casu, L. Tută, I. Nicolaescu, and C. Moraru, "Some aspects about the advantages of using MIMO systems," in *2014 22nd Telecommunications Forum Telfor (TELFOR)*, 2014, pp. 320–323.

[17] A. Argyriou, "Preventing Carrier Acquisition from Unauthorized Wireless Communication Receivers," 2020.

[18] A A , "ECE511 Π Θ T Σ ." [Online]. Available: https://www.e-ce.uth.gr/

[19] A. Pirsiavash and M. J. Emadi, "Rician channel characterization in OFDM systems," in *2015 23rd Iranian Conference on Electrical Engineering*, 2015, pp. 303–307.

[20] J. D. Schreuder, "QAM CARRIER TRACKING FOR SOFTWARE DEFINED RADIO," in *SDR '08 Technical Conference and product Exposition*, 2008.

[21] N. V. Kuznetsov, J. Ladvanszky, M. V. Yuldashev, and R. V. Yuldashev, "PLL and Costas loop based carrier recovery circuits for 4QAM: non-linear analysis and simulation," 2018.

[22] A. V. Oppenheimer and R. W. Schafer, *Ψ E Σ T E* . Fountas, 2013.

[23] (2008) Carrier Acquisition and Tracking. [Online]. Available: https://my.ece.utah.edu/~ece6590/ch9.pdf

[24] (2018) Phase Locked Loop (PLL) in a Software Defined Radio (SDR). [Online]. Available: https://wirelesspi.com/phase-locked-loop-pll-in-a-software-defined-radio-sdr/

[25] A. V. Oppenheimer, A. S. Willsky, and S. H. Nawab, *Σ Σ Δ E* . Fountas, 2012.

[26] A A , "ECE312 T Σ ." [Online]. Available: https://www.e-ce.uth.gr/

[27] K A , "ECE555 Π Θ Δ ." [Online]. Available: https://www.e-ce.uth.gr/